Chapter 4

4.1 Introduction

In this chapter, we have discussed the structural transformation in $GdMnO_3$ after increasing Fe concentration (x) from 0.3 to 0.5. Microstructure is described in section 4.2.1. Structural parameters obtained from Rietveld refinement are tabulated and are discussed in section 4.2.2. Raman, photoluminescence and XPS spectra are analyzed and are discussed in section 4.2.3, 4.2.4 and 4.2.5, respectively. Section 4.3 describes the magnetic properties. Conclusions of this chapter are discussed in section 4.4.

4.2 Structural, Microstructural and Optical Analysis

The surface morphology with particle size using the SEM data is discussed in section 4.2.1. The structural transformation and the decrement in J-T distortion using the lattice constants and bond lengths which are obtained from Rietveld refinement of XRD data is discussed in section 4.2.2. The decrement in J-T distortion is further confirmed through Raman spectra and photoluminescence spectroscopy given in section 4.2.3 and 4.2.4, respectively.

4.2.1 Scanning Electron Microscopy

In order to realize the shape and size of particles, the field emission scanning electron (FE-SEM) micrographs of $GdMn_{1-x}Fe_xO_3$ (x = 0.3 and 0.5) are shown in **figure 4.1**. Micrographs indicate the semi spherical agglomerated particles having size ranging from 100-200 nm.

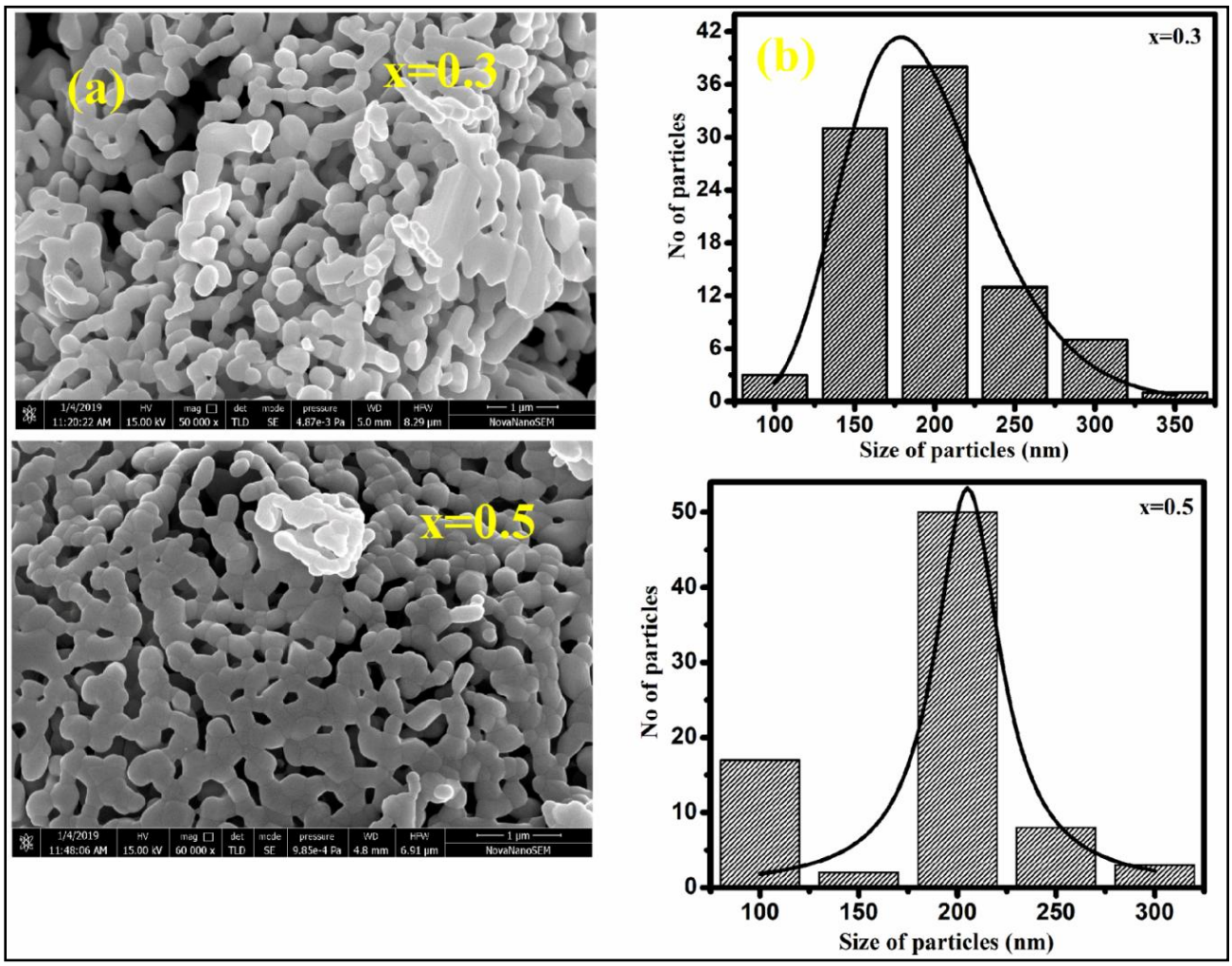

Figure 4.1 *Field emission scanning electron micrographs of* $GdMn_{1-x}Fe_xO_3$ *(x = 0.3 and 0.5).*

4.2.2 Rietveld refinement of XRD patterns and J-T distortion

Figure 4.2 depicts the Rietveld refinement of the powder XRD Fe doped $GdMn_{1-x}Fe_xO_3$ (x = 0.3 and 0.5) samples. In order to grasp the structural evolution in $GdMnO_3$ after Fe doping, XRD patterns are fitted using Rietveld refinement method of FULLPROF programme considering Pseudo-Voigt function. We observe that although both compounds

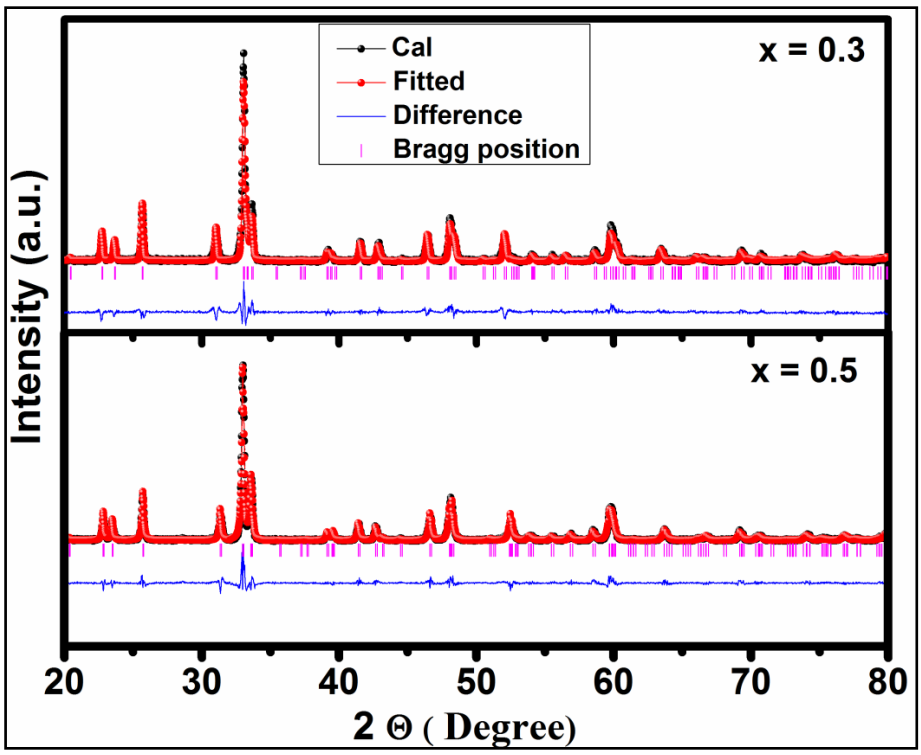

Figure 4.2 *X-ray diffraction (XRD) patterns of $GdMn_{1-x}Fe_xO_3$ (x = 0.3 and 0.5) fitted using Rietveld refinement of Fullprof programe.*

are crystallized in orthorhombic structure, while lattice parameters a and c expand, b shows a contraction with increasing '*x*' from 0.3 to 0.5 (**Table 4.1**). Being an orthorhombic structure, the lattice parameters can be expressed as a ≈ b ≈ c/√2. When a< c/√2<b, the structure is said to be O type orthorhombic and for O' orthorhombic, the condition is c/√2<a<b. In the present case, we have found that for *x* = 0.3, O' structure transforms to O type when *x* = 0.5. Similar O' to O type transformation has also been reported in case of K doped $NdMnO_3$ [84]. From Rietveld refinement, we have noticed that the lattice volume decreases from 230.41 to 229.91 $Å^3$ with an increase in x from 0.3 to 0.5. The decrease inlattice volume with '*x*' could be due to replacement of Fe^{3+} at Mn^{3+} site in $GdMnO_3$. In perovskite containing Fe^{3+} and Mn^{3+}, the crystal field splitting is smaller than the Hund's

Table 4.1 *Structural Parameters of $GdMn_{1-x}Fe_xO_3$ (x= 0.3 and 0.5) at room temperature revealed from the Rietveld structure refinement.*

Parameters	**x= 0.3**	**x= 0.5**
a(Å)	5.3227(4)	5.3284(4)
b(Å)	5.7579(4)	5.7011(4)
c(Å)	7.5181(4)	7.5678(4)
α, β, ϒ		
V($Å^3$)	230.41	229.91
Gd(x, y, z)	(0.9846(4),0.0749(4),0.25)	(0.9804(4),0.0722(4),0.25)
Mn/Fe (x, y, z)	(0.5,0,0)	(0.5,0,0)
O1 (x, y, z)	(0.1015(3),0.4652(3),0.25)	(0.1004(3),0.4702(3),0.25)
O2 (x, y, z)	(0.7059(3),0.3099(3),0.0486(3)	(0.7097(3),0.3033(3),0.0583(3)
χ^2	2.12	2.77
Mn-O1(Å)	1.96	1.99
Mn-O2 (Å)(l)	2.13	2.08
Mn-O2' (Å)(s)	1.94	1.95
Mn-O1-Mn(deg)	146.0	144.24
Mn-O2-Mn(deg)	148.7	150.48
|a-b|	0.4352	0.3719

energy between two electrons [85] and thus, Fe and Mn ions are in the high spin state. The ionic radius in high spin state for both Fe and Mn in 6 coordination are equal i.e. 0.64 Å.

Thus the decrease in lattice volume could not be ascribed to the replacement of Mn^{3+} with Fe^{3+}. The other possibility could be the presence of Fe^{2+} or Mn^{4+}. The ionic radius of Fe^{2+} in high spin state is 0.78 Å, which is higher than Mn^{3+}/Fe^{3+} ions. However, the ionic radius of Mn^{4+} is 0.53 Å, which is less than Fe^{2+}, Fe^{3+} and Mn^{3+}. Thus the decrease in lattice volume is attributed to the presence of Mn^{4+} which leads to reduction in Mn-O bond length. Thus the reduction in bond length diminishes the volume of the MnO_6 octahedra and hence decreases the lattice volume. The presence of Mn^{4+} is further confirmed from XPS which we have discussed later.

The 3D crystal structure of $GdMn_{1-x}Fe_xO_3$ (x = 0.3 and 0.5) generated from the refined structural parameters including atomic positions using Vista software are shown in **figure 4.3**. The two apical positions of the MnO_6 octahedra are occupied by O1 atoms (red balls) whereas the four equatorial positions are occupied by the O2 atoms (green balls) (**figure. 4.3**). The equatorial Mn-O2 bonds are shown in **figure. 4.4** have two different bond lengths. A small change in bond length Mn-O and bond angle Mn-O-Mn change the J-T distortion and the degree of tilting of octahedra. One can notice that Mn-O bond length is not symmetrical. Rather show two different bond lengths, one is short and other is long. But in an undistorted octahedra, one may expect the average Mn–O bond length close to the sum of ionic radii of manganese (r_{Mn}) and oxygen (r_o) i.e. 1.93 Å. The deviations in Mn–O bond length from1.93 Å along different directions reveal a strong J-T distortion. The J-T distortion is calculated using the following empirical relation [87],

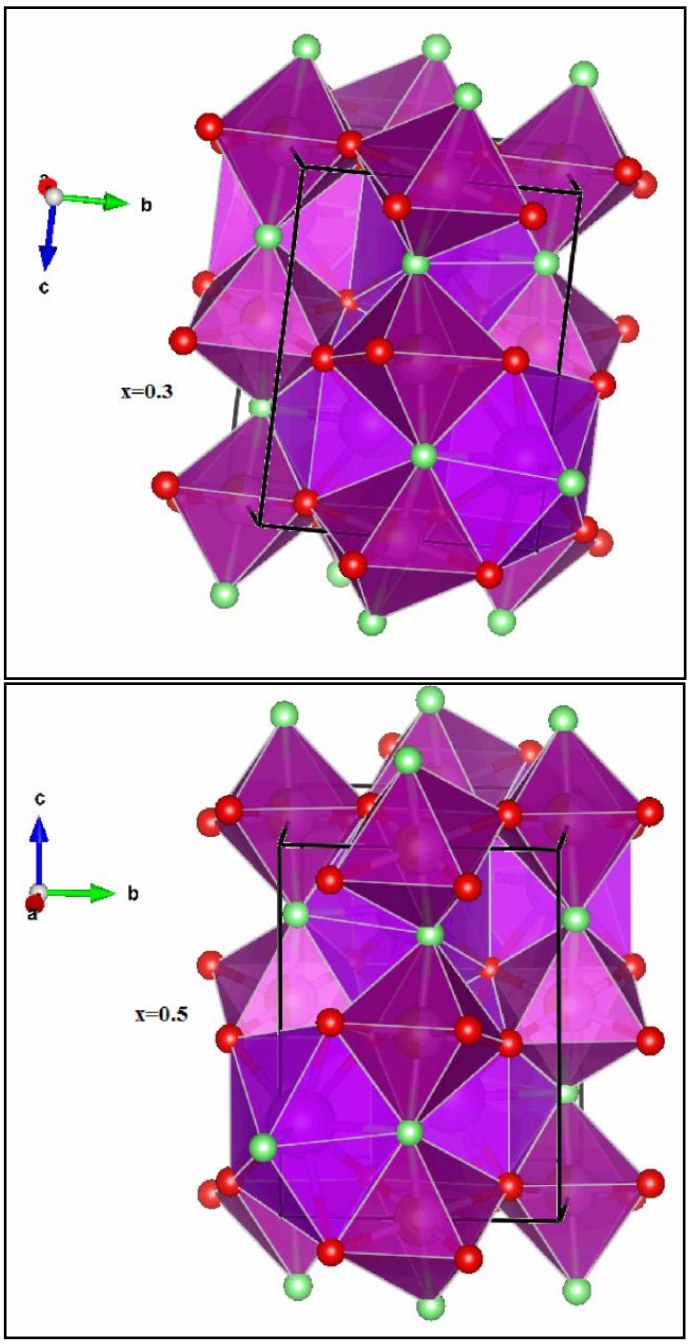

Figure 4.3 *Crystal structure obtained from Rietveld refinement drawn using Vesta software of* $GdMn_{1-x}Fe_xO_3$ *(x = 0.3 and 0.5).*

$$\sigma_{JT} = 1/3\Sigma_i[(Mn\text{-}O)_i - \langle Mn\text{-}O\rangle]^{1/2} \quad (1)$$

where, Mn-O and average $\langle Mn\text{-}O\rangle_i$ bond lengths are calculated from Rietveld refinement as shown in Table 1. The J-T distortion factor decreases from 0.08 to 0.06 when increasing

x from 0.3 to 0.5. The average angular distortion ($\omega = 180^{o} - \langle\Theta\rangle$) due to tilting of MnO_6 decreases from 34.88^{o} to 30.41^{o} when x increases from 0.3 to 0.5. Thus Fe substitution converts the distorted orthorhombic structure to a more symmetrical one. Further, decrease in the difference of lattice parameters (|a-b|) with x demonstrates a higher structural symmetry i.e. a tetragonal unit cell [84]. The evidence of J-T distortion is further examined from Raman measurements.

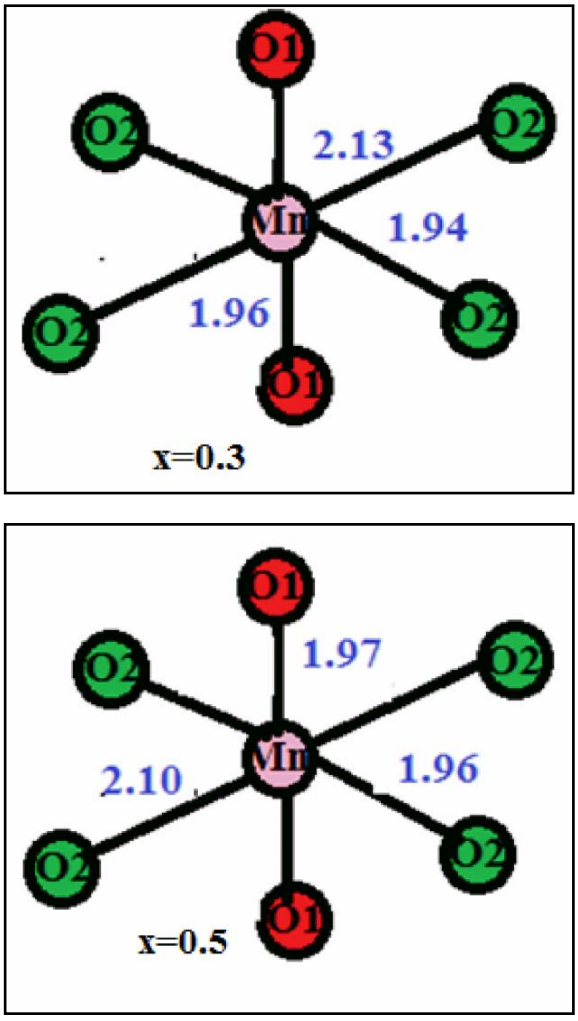

Figure 4.4 *Bond- lengths obtained from Rietveld refinement drawn using Vesta software of* $GdMn_{1-x}Fe_xO_3$ *(x = 0.3 and 0.5).*

4.2.3 Raman Spectroscopy

In perovskites with *Pbnm* structure, the Raman active modes are $7A_g + 7B_{1g} + 5B_{2g} + 5B_{3g}$ [22]. These modes are active due to the deviations in the ideal perovskite structure. Raman spectra of $GdMn_{1-x}Fe_xO_3$ (x= 0.3 and 0.5) at room temperature are shown in **figure. 4.5**. From the spectra we have observed raman modes at 370, 487 and 610 cm^{-1}. Out of these three modes, while the Raman peak at 487 cm^{-1} is attributed to A_g mode arising from in-plane antisymmetric vibration of O2, B_{2g} mode at 610 cm^{-1} is assigned to in-plane stretching of O2 [99]. Both the peaks are correlated to J-T distortion. The intensity of peak observed at 487 cm^{-1} in x=0.3 is found to be almost disappeared and the intensity of peak at 610 cm^{-1} is reduced when x=0.5. The other two vibrational modes at 370 cm^{-1} is assigned to tilting of MnO_6 octahedra [[22],[88]]. Although the frequency of the Raman band due to octahedral tilting although does not change, the intensity of the band is found to reduce with increase in Fe concentration. We have further studied J-T distortion induced structural changes by means of photoluminescence spectra.

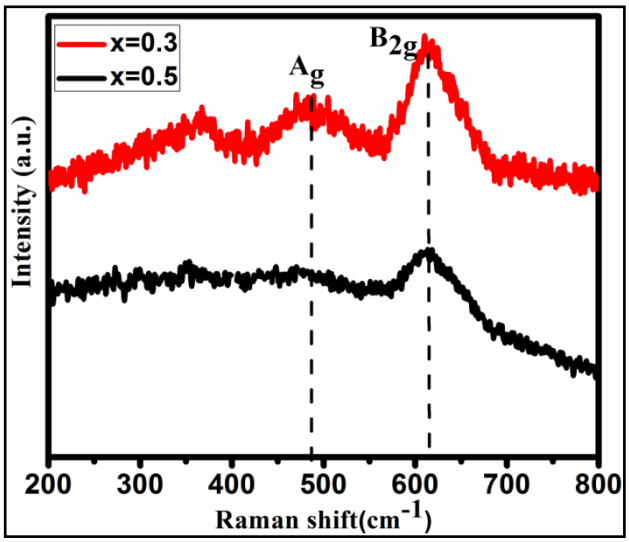

Figure 4.5 Raman spectra of $GdMn_{1-x}Fe_xO_3$ (x = 0.3 and 0.5).

4.2.4 Photoluminescence Properties

The emission spectra of $GdFe_xMn_{1-x}O_3$ (x = 0, 0.3 and 0.5) in the spectral range of 270-370 nm and 420-570 nm obtained under an excitation wavelength of 200 nm are shown in **figure 4.6**. For x = 0, within 270-370 nm spectral region, PL spectra consist of a broad emission band (~270-300 nm) with peaks centered at ~286 and 308 nm along with other two intense peaks at 336 and 353 nm (see right panel of **figure 4.6**). Interestingly, the emission peak at ~286 nm shown with shaded area is found to be absent for x = 0.3 and 0.5. We have estimated J-T distortion factor as 0.2 for $GdMnO_3$ which decreases to 0.08 and 0.06 for x = 0.3 and 0.5, respectively. Thus, the disappearance of emission peak at ~286 nm is accompanied with the significant reduction in J-T distortion factor from 0.2 to 0.06. In

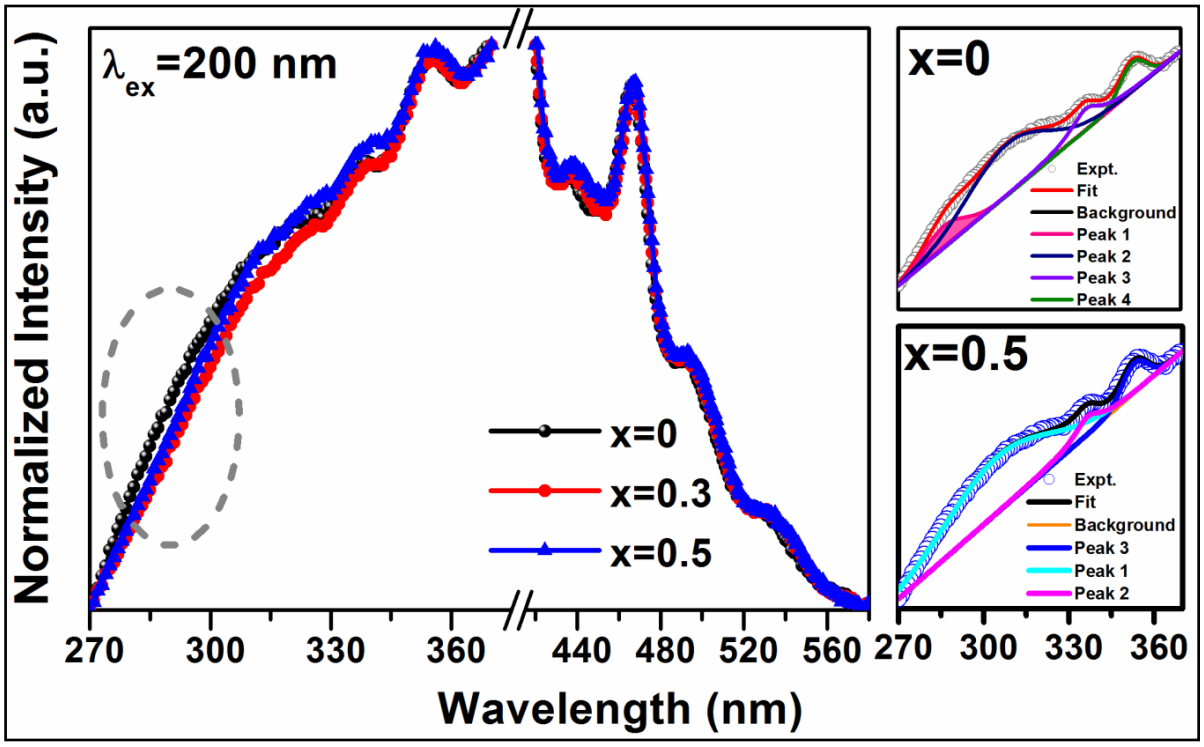

Figure 4.6 *Room temperature emission spectra of $GdMn_{1-x}Fe_xO_3$ (x = 0, 0.3 and 0.5) at an excitation wavelength 200 nm.*

this context, Moreira *et al*. observe that PL emission peak can vanish in a similar highly crystalline $CaTiO_3$ system primarily comprised of undistorted or ordered TiO_6 clusters [100].

The higher spectral range from 420 to 570 nm demonstrates the intense emission peak at ~466 nm together with broad shoulder bands at 439, 495 and 535 nm. No significant change in intensity and/or position of emission peaks is observed with change in Fe concentration. In our XPS analysis, we have the evidences for coexistence of Mn^{3+} and Mn^{4+} ions. In case of Mn^{3+}, it is known that local charge transfer energy band usually splits under the influence of J-T distortion and crystal field energy. Therefore, four distinct charge transfer bands are produced such as 3.5, 4, 8 and 8.5 eV arising due to transition of electrons from O *2p* → Mn(t_{2g}−JT), Mn(t_{2g} + JT), Mn(e_g−JT) and Mn(e_g + JT), respectively [[46],[47]]. On the other hand, Mn^{4+} energy levels are realized according to Tanabe–Sugano diagram for $3d^3$ configurations in an octahedral symmetry. The spin allowed electronic transitions are observed when electrons move from higher energy states such as ^2E_g, $^4T_{2g}$, $^2T_{2g}$ and $^4T_{1g}$ etc to ground state $^4A_{2g}$ [48]. The broad emission peaks within 270-370 nm spectral range are assigned to $^4T_{1g} \rightarrow {}^4A_{2g}$ electronic band transition whereas the highest intensity peak at ~466 nm along with 439 nm originates from $^2T_{2g} \rightarrow {}^4A_{2g}$ electronic transition. The broad-ranging emissions from 500-535 nm are attributed to partial decay of electrons from $^4T_{2g}$ to $^4A_{2g}$ [48]. It is noteworthy that the distinct energy levels of Mn^{3+} exist within close proximity of Mn^{4+} energy levels. It suggests the possibility of overlapping of different energy levels and thus the transfer of electrons from Mn^{3+} to Mn^{4+} which contributes to emission spectra cannot be ruled out completely.

After monitoring the highest emission peak at ~466 nm, the excitation spectra of $GdFe_xMn_{1-x}O_3$ (x=0, 0.3 and 0.5) have been taken as depicted in **figure 4.7**. The excitation spectrum of $GdMnO_3$ primarily exhibits a broad excitation band ranging from 310-390 nm with maximum at ~370 nm and other sharp peaks at 398 and 406 nm. While the former broad band is ascribed to excitation of electrons from $^4A_{2g}$ to lower of $^4T_{1g}$ energy level, transition of electrons from $^4A_{2g}$ to upper of $^2T_{2g}$ gives rise to excitation peaks at 398 and 406 nm [[48],[101]]. For x=0.3, the intensity of excitation peaks (398 and 406 nm) increases significantly and become sharp while the peak positions remains same. In case of x=0.5, the intensity of excitation peaks diminishes slightly showing nearly similar spectrum.

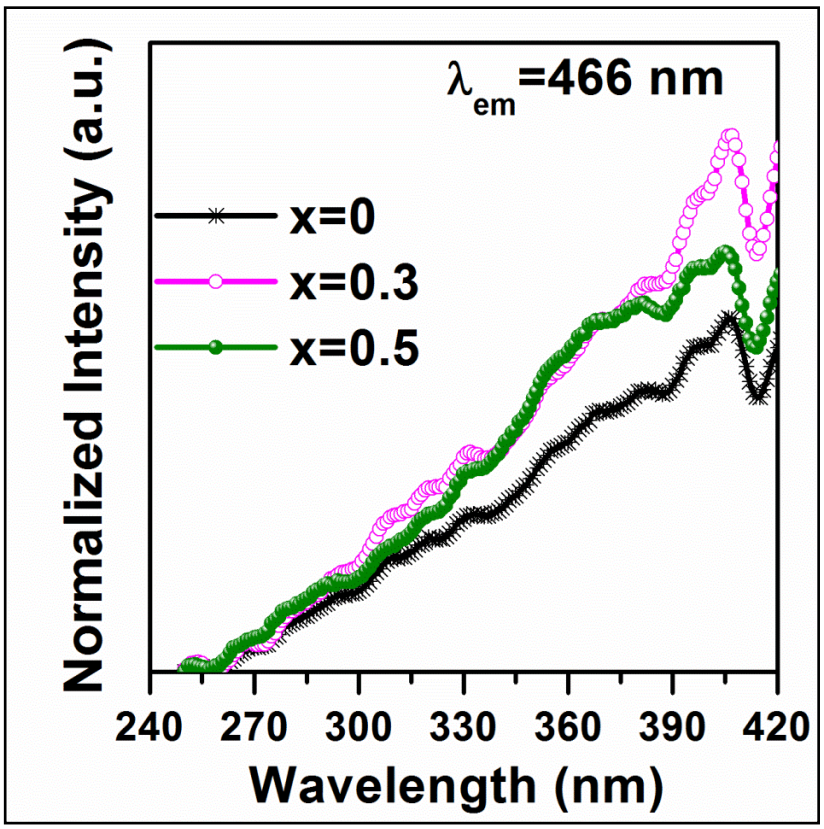

Figure 4.7 *Room temperature excitation spectra of* $GdMn_{1-x}Fe_xO_3$ *(x = 0, 0.3 and 0.5) at an emission wavelength 466 nm.*

Combining different photoluminescence properties, we propose an energy level diagram (**figure 4.8**) to demonstrate possible electronic transitions involved in $GdFe_xMn_{1-x}O_3$. In such systems, photoluminescence properties are observed essentially due to electronic transitions within *d-d* energy bands. We have designated various probable energy bands such as O *2p*, Mn(t_{2g}–JT), Mn(t_{2g} + JT), Mn(e_g–JT), Mn(e_g + JT) of Mn^{3+} and ^2E_g, $^4T_{2g}$, $^2T_{2g}$, $^4T_{1g}$, $^4A_{2g}$ associated to Mn^{4+}, respectively. Under an excitation wavelength of 200 nm (~6.2 eV), the electrons residing at O *2p* and $^4A_{2g}$ levels do not get excited to higher energy states Mn(e_g–JT) and Mn(e_g + JT).

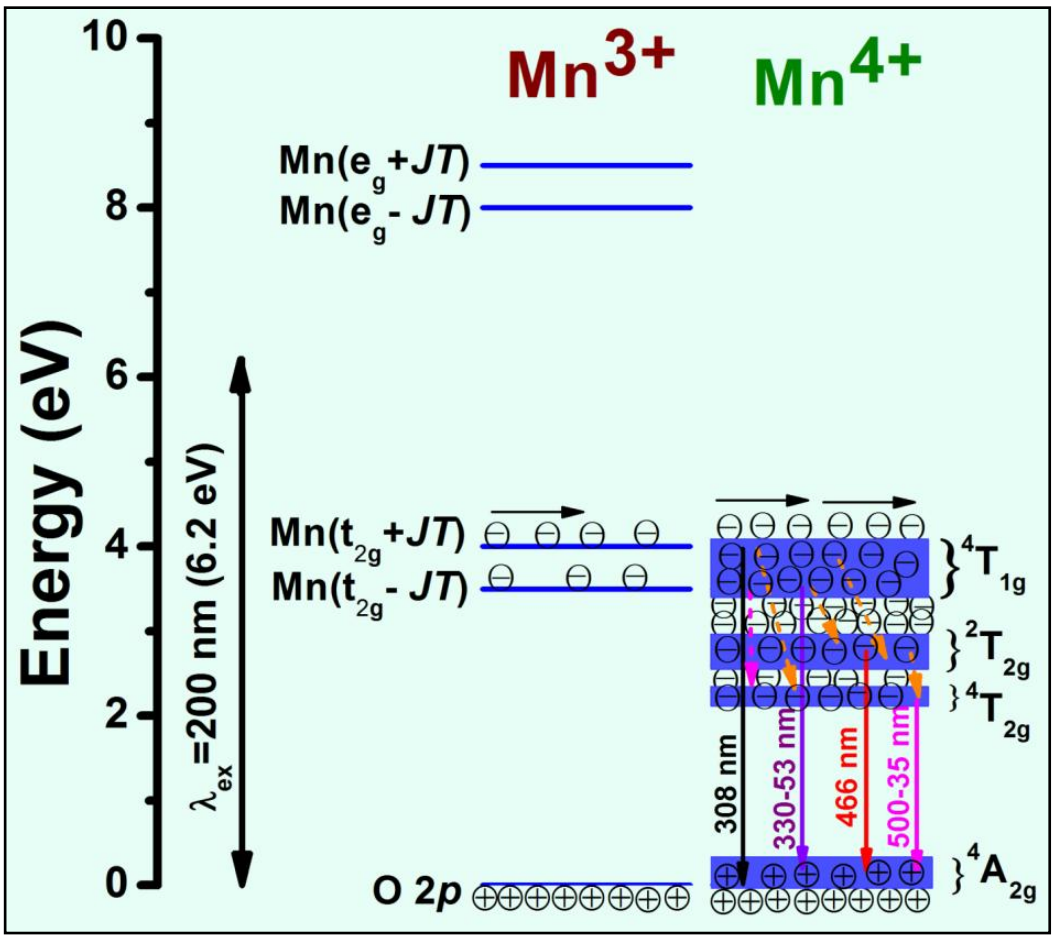

Figure 4.8 *Energy band diagram of* $GdMn_{1-x}Fe_xO_3$ *(x = 0.3 and 0.5).*

After absorbing incident pumping energy, energetic electrons are transferred to high energy level, $^4T_{1g}$ and $^2T_{2g}$ of Mn^{4+}. Considering the fact that energy levels of Mn^{3+} and Mn^{4+} are closely present, a few number of electrons can be expected to get excited to higher levels e.g. Mn(t_{2g}−JT) and Mn(t_{2g} + JT). However, there is an abundance of excited electrons at $^4T_{1g}$ and $^2T_{2g}$ energy levels of Mn^{4+}. When the excited electrons situated at $^4T_{1g}$ relax directly to ground state, $^4A_{2g}$, a broad emission band in spectral range of 270-370 nm is observed. Most of the electrons decay and get populated at $^2T_{2g}$ and $^4T_{2g}$ energy levels which eventually de-excited to $^4A_{2g}$ producing intense emission peak at ~466 nm and 500-535 nm broad band emission.Most of the electrons decay and get populated at $^2T_{2g}$ and $^4T_{2g}$

energy levels which eventually de-excited to $^4A_{2g}$ producing intense emission peak at ~466 nm and 500 to 535 nm broad band emission.

4.2.5 X-ray Photoelectron Spectroscopy

XPS of $GdMn_{1-x}Fe_xO_3$ (x = 0.3 and 0.5) collected using Al K_α radiation are depicted in **figure 4.9, 4.10 and 4.11**. The core level binding energies are aligned with the carbon binding energy of 284.6 eV. The Manganese $2p_{3/2}$ core level spectra are asymmetric in nature showing maximum binding energy peak at 641.6 eV. The asymmetric peak of Mn is fitted with two Gaussian peaks using XPS peak 4.1 software with Shirley background. The two components observed at ~641.3 and ~642.8 eV correspond to Mn^{3+} and Mn^{4+}, respectively. The existance of Mn^{4+} ions endorses the decrease in lattice volume observed from Rietveld refinement. The asymmetric peak of Mn, Fe and O are fitted with mixed Gaussian and Lorentzian functions using XPS peak 4.1software. The two components observed at ~641.3 and ~642.8 eV corresponds to Mn^{3+} and Mn^{4+}, respectively (**figure 4.9**). The peaks in Fe spectra at ~710 and ~713 eV correspond to Fe^{2+} and Fe^{3+}, respectively (**figure 4.10**). The O 1*s* core level spectra of oxygen shown in **figure 4.11** appear asymmetric around ~529 eV. Therefore, the spectra are fitted with mixed Gaussian and Lorentzian functions denoted as O_a and O_b using the aforementioned software for x = 0.3 and 0.5. While O_a peak located at 529 eV is ascribed to the lattice oxygen atoms, O_b peak centered at ~531 eV is due to the presence of oxygen vacancies.A small peak appears in x = 0.5 at ~532 eV originates partly from the hydroxyl groups and from the chemisorbed oxygen lying on the surface of the samples [102]. Further, from XPS spectra of Fe 2*p*, Mn 2*p* and O 1*s*, the estimated area ratios of Mn^{4+}/Mn^{3+} and Fe^{2+}/Fe^{3+} increases whereas Ob/Oa area ratio decreases with increasing Fe concentration. The decrease in oxygen

vacancies confirms that Mn^{4+} dominates over Fe^{2+}. Hence, we establish that the lattice volume is decreased with Fe concentration due to Mn^{4+}.

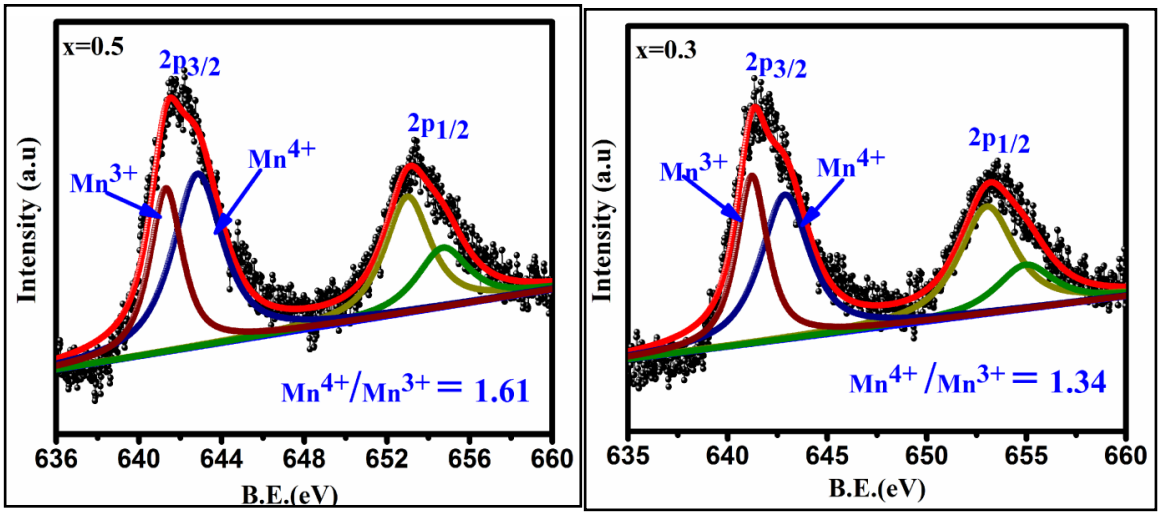

Figure 4.9 *X-ray photoelectron spectroscopy for Mn 2p of* $GdMn_{1-x}Fe_xO_3$ *(x = 0.3 and 0.5).*

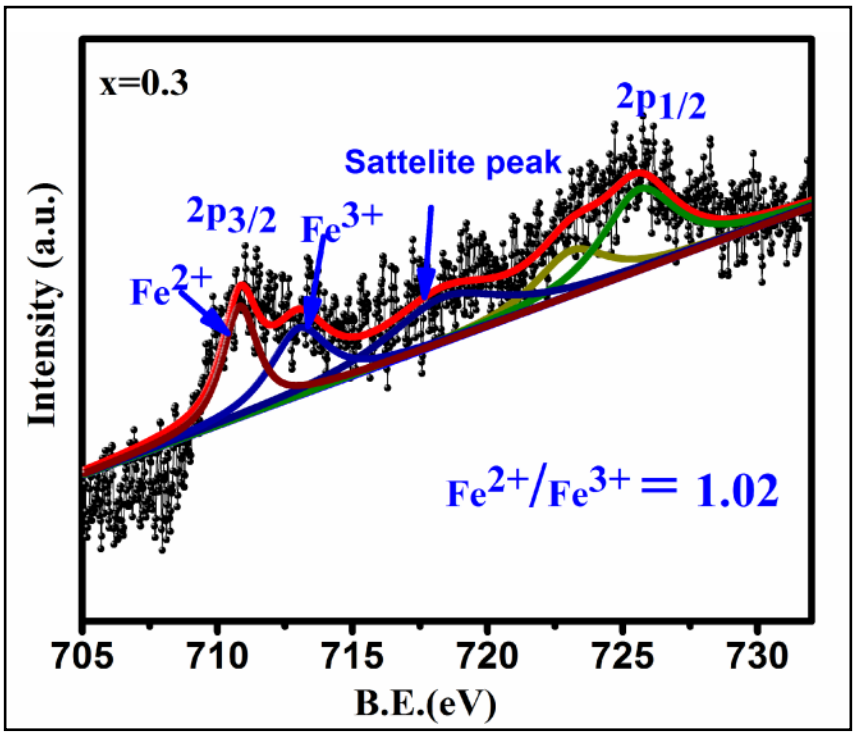

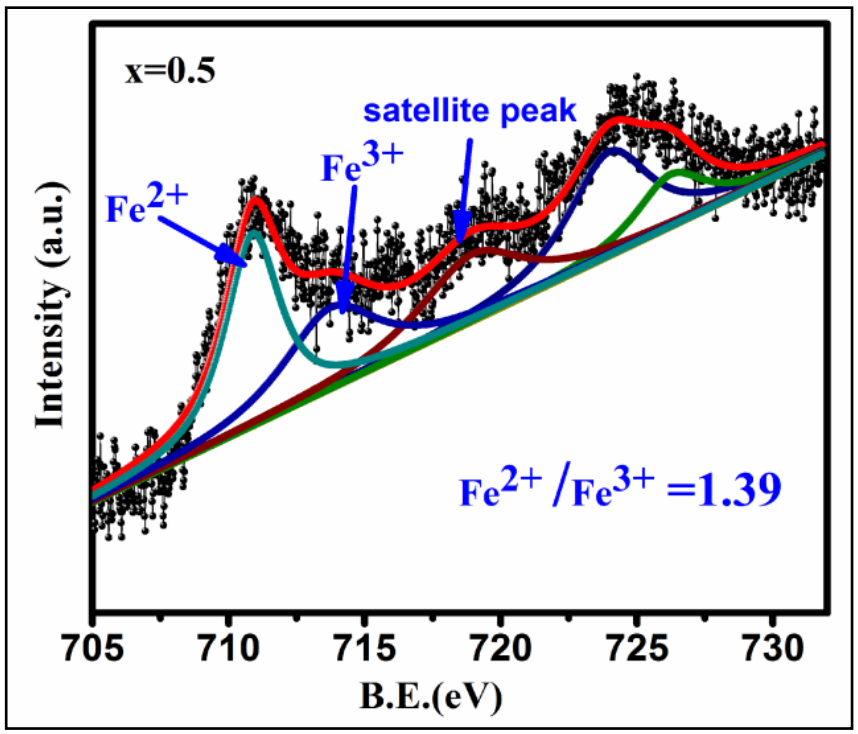

Figure 4.10 *X-ray photoelectron spectroscopy for Fe 2p of* $GdMn_{1-x}Fe_xO_3$ *(x = 0.3 and 0.5).*

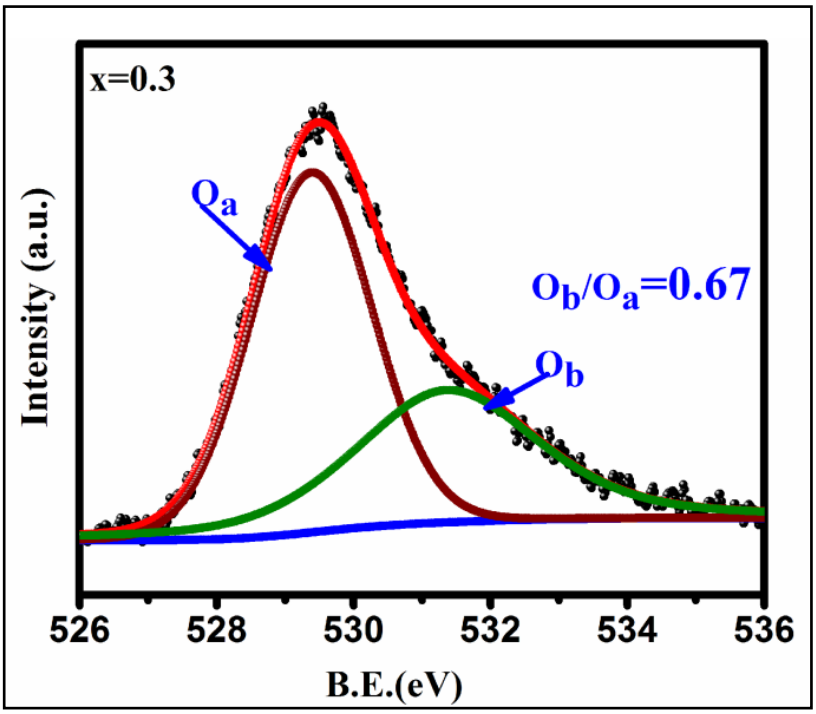

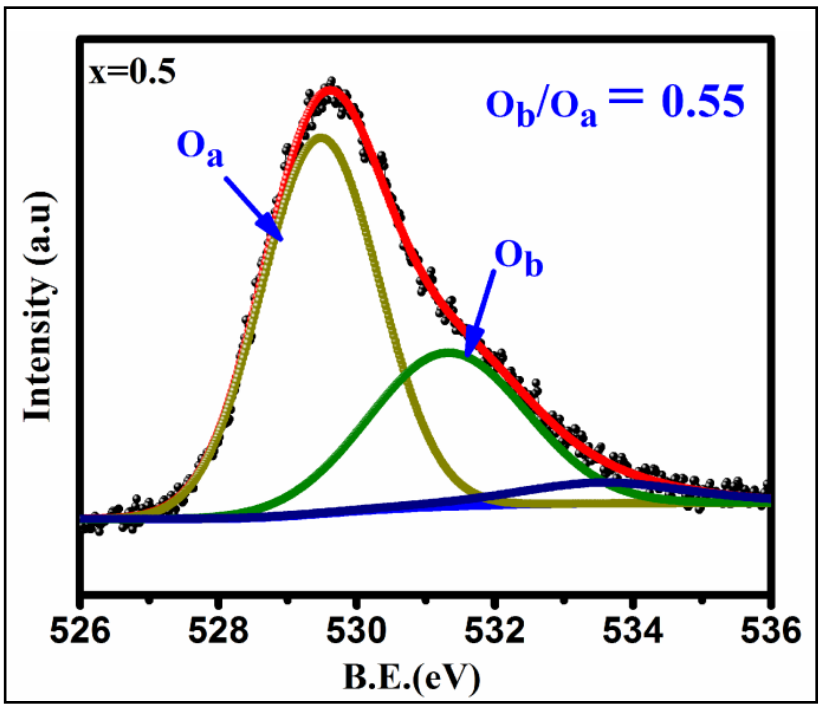

Figure 4.11 *X-ray photoelectron spectroscopy for O1s of* $GdMn_{1-x}Fe_xO_3$ *(x = 0.3 and 0.5).*

4.3 Magnetic Properties

To study the magnetic properties after Fe doping in $GdMnO_3$, the temperature dependent magnetization, magnetic field dependent magnetization, temperature dependent ac susceptibility and time dependent magnetization are carried out and are discussed in 4.3.1, 4.3.2, 4.3.3 and 4.3.4, respectively.

4.3.1 Temperature dependent magnetization

The temperature dependent magnetization of $GdMn_{1-x}Fe_xO_3$ (x = 0.3 and 0.5) in zero-field-cooled (ZFC) and field-cooled (FC) conditions at 0.05 and 10 kOe external magnetic field is shown in **figure 4.12**. With decreasing temperature from 300 K, a clear bifurcation of FC and ZFC magnetization curves has been observed at a temperature which is known to be T_N. Further decreasing temperature, magnetization shows an anomaly at ~

9.8 K with a maxima at T_{max} ~ 3.5 K in x = 0.3 compound which is not clear in x = 0.5 compound. At 10 kOe, bifurcation observed in FC and ZFC magnetization disappears showing no thermomagnetic irreversibility (**figure. 4.13)**. This is appropriate to the fact that at high magnetic field, all moments can align themselves along the field direction. In order to deduce the magnetic anomalies in $GdMn_{1-x}Fe_xO_3$, we have shown $1/\chi$ vs T measured at 0.05 kOe in **figure 4.14**. A clear bifurcation is observed in x =0.5. T_N in case of x = 0.5 is observed at ~298 K. Since T_N is not explicitly realized from $1/\chi$ vs T plot for x = 0.3, we have estimated T_N by plotting M_{FC}-M_{ZFC}/M_{ZFC} as a function of temperature shown in **figure 4.15**. T_N is found to be ~ 286 K for x = 0.3. T_N is the temperature at which the transition from paramagnetic to antiferromagnetic phase takes place. Besides T_N, with decreasing temperature **figure 4.15**, it is observed that the magnetization falls steadily which is attributed to spin reorientation transition (T_{SR}) in a particular plane.

T_{SR} is found to be ~270 and ~253 K for x = 0.3 and 0.5, respectively. Although Pal *et al*. have shown T_{SR} from M_{FC} vs Temperature plot for $GdMn_{1-x}Fe_xO_3$ ($0.4 \leq x \leq 0.7$) [31]], interestingly, we could capture T_{SR} at ~270 K for x = 0.3, which has not been observed earlier [31]]. From $1/\chi$ vs T, towards low temperature regime (**figure 4.14**), the two magnetic

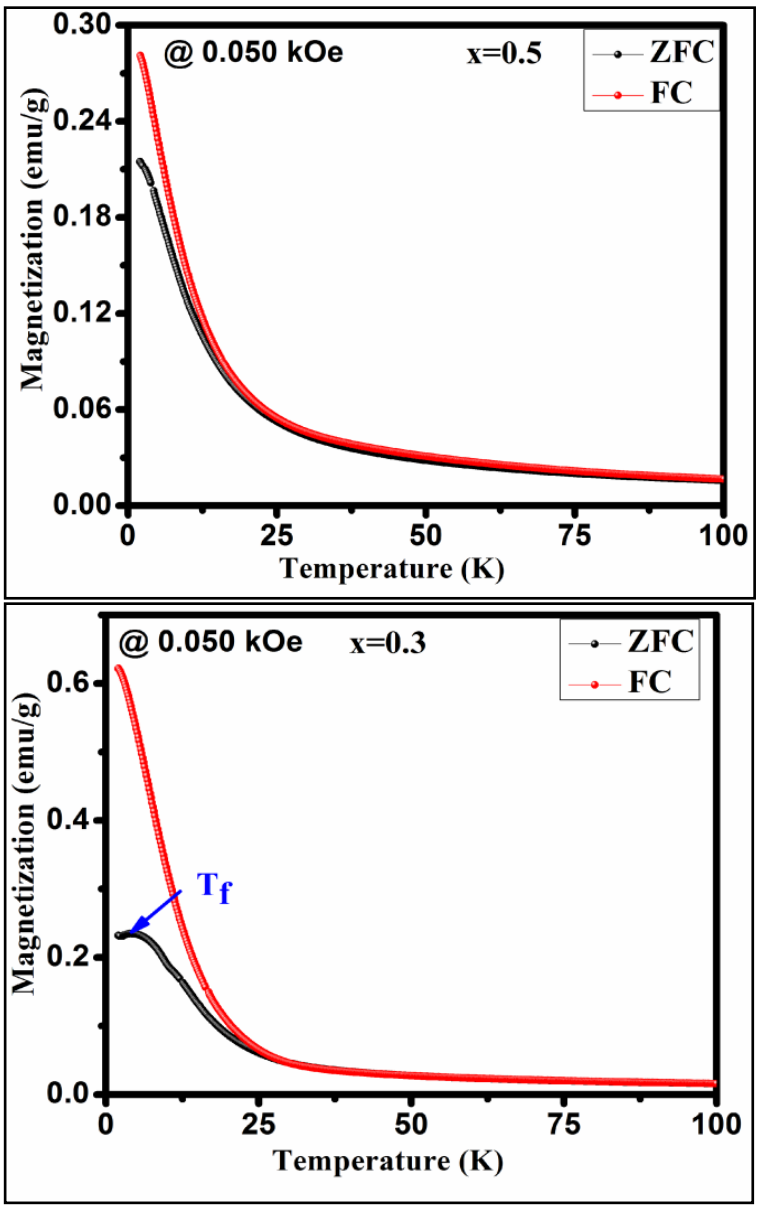

Figure 4.12 *Temperature dependent magnetization under zero field cooling (ZFC) and field cooling (FC) measured at 0.050 kOe for* $GdMn_{1-x}Fe_xO_3$ *(x = 0.3 and 0.5).*

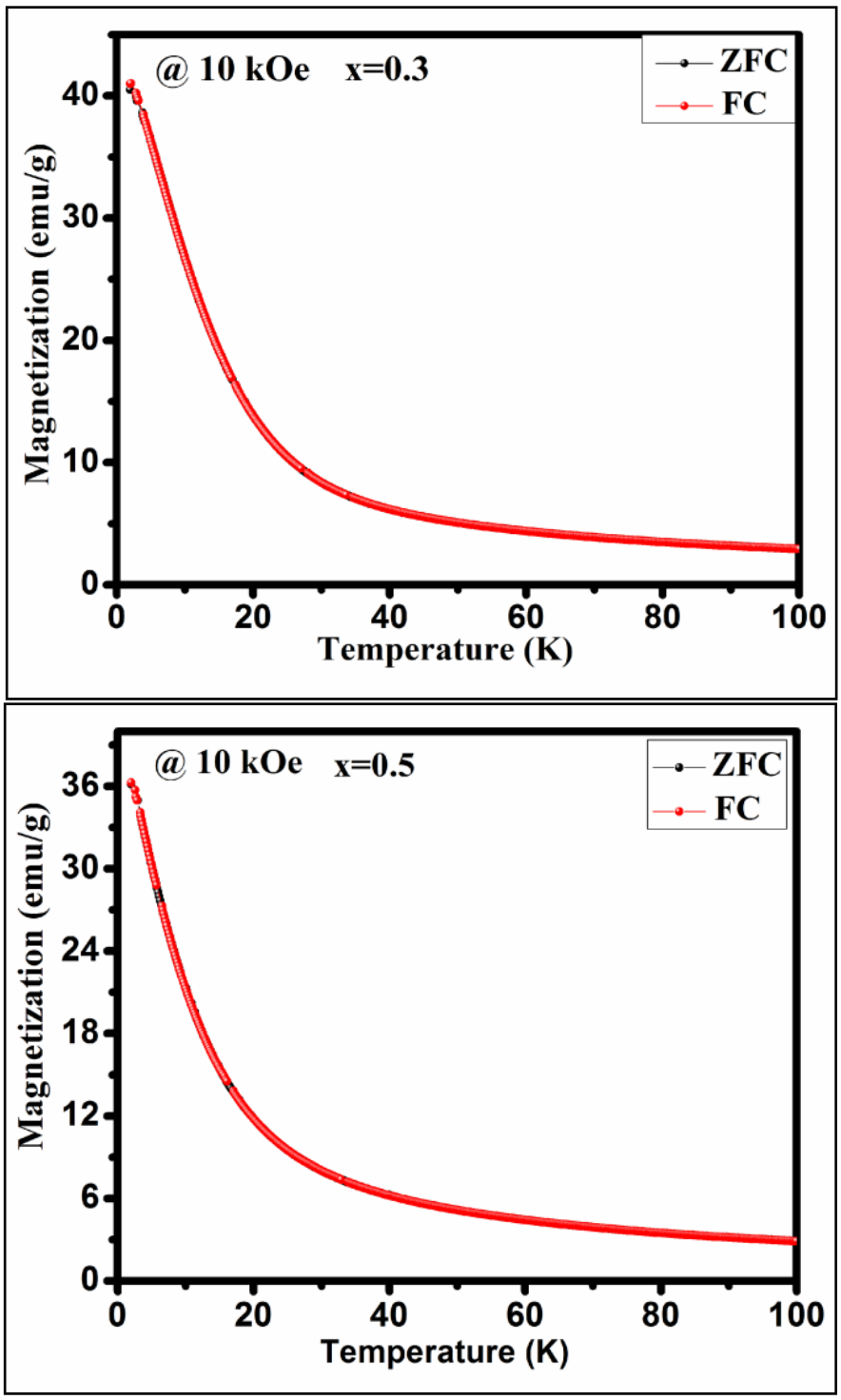

Figure 4.13 *Temperature dependent magnetization under zero field cooling (ZFC) and field cooling (FC) measured at 10 kOe for* $GdMn_{1-x}Fe_xO_3$ *(x = 0.3 and 0.5).*

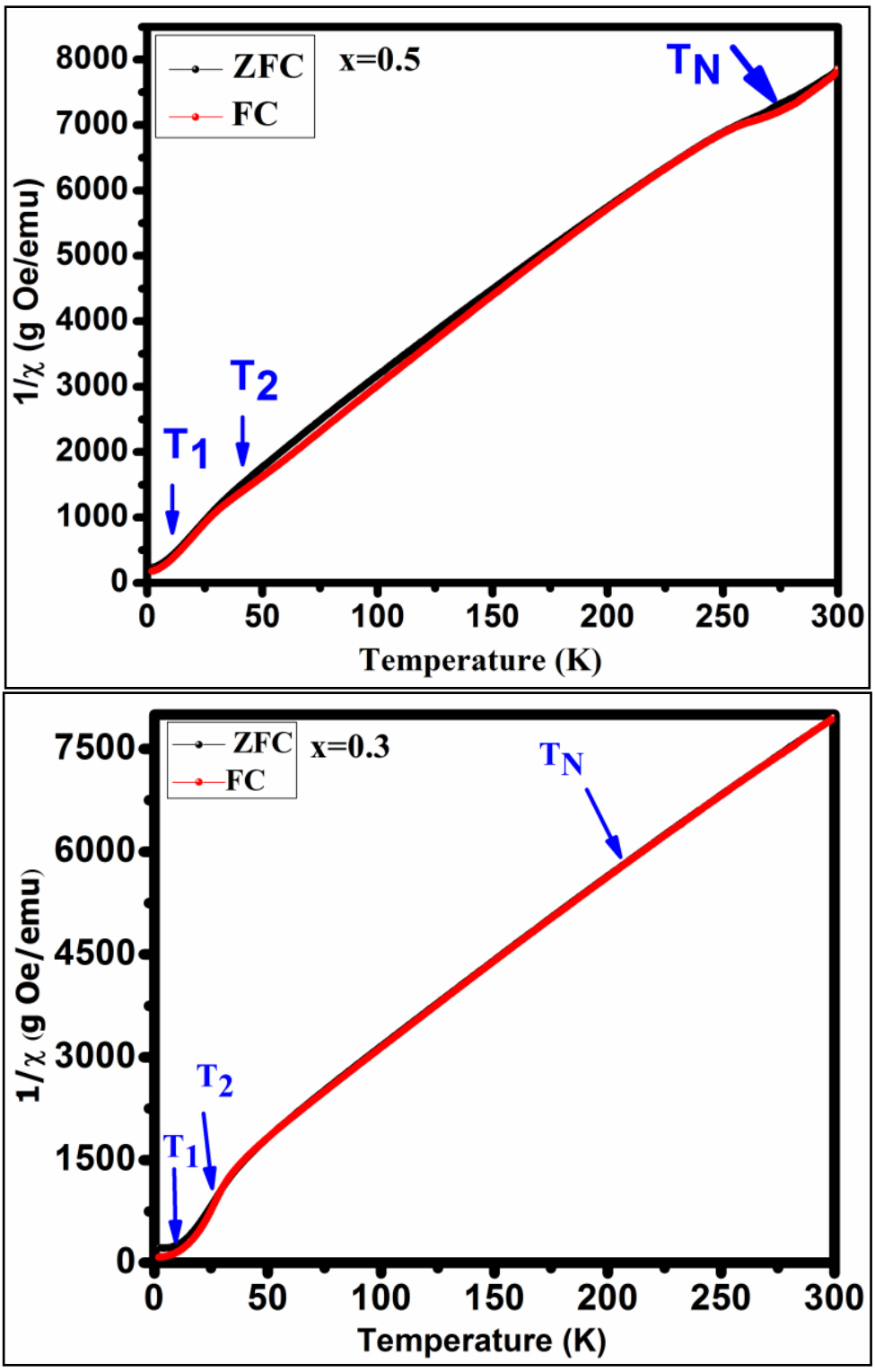

Figure 4.14 *The inverse susceptibility,1/χ plots of ZFC and FC in the presence of 0.050 kOe of x = 0.3 and 0.5.*

anomalies T_1 and T_2 are observed at ~22 and ~5 K, respectively for pristine sample. In case of x = 0.3, T_1 is shifted to ~34 K followed by shifting of T_2 to ~9.8 K. It is noted that at x = 0.5, the position of T_2 remains same whereas T_1 approaches ~37 K. The anomalies at ~22 and ~5 K are revealed due to the canted AFM ordering of Mn^{3+} and ordered Gd^{3+} spins, respectively. To deduce the magnetic anomalies in $GdMn_{1-x}Fe_xO_3$, we have shown $1/\chi$ vs T measured at 0.05 kOe in **figure 4.14**. With decreasing temperature from 300 K, at around ~34 K, magnetization suddenly decreases showing a kink at ~ 9.8 K when x = 0.3.

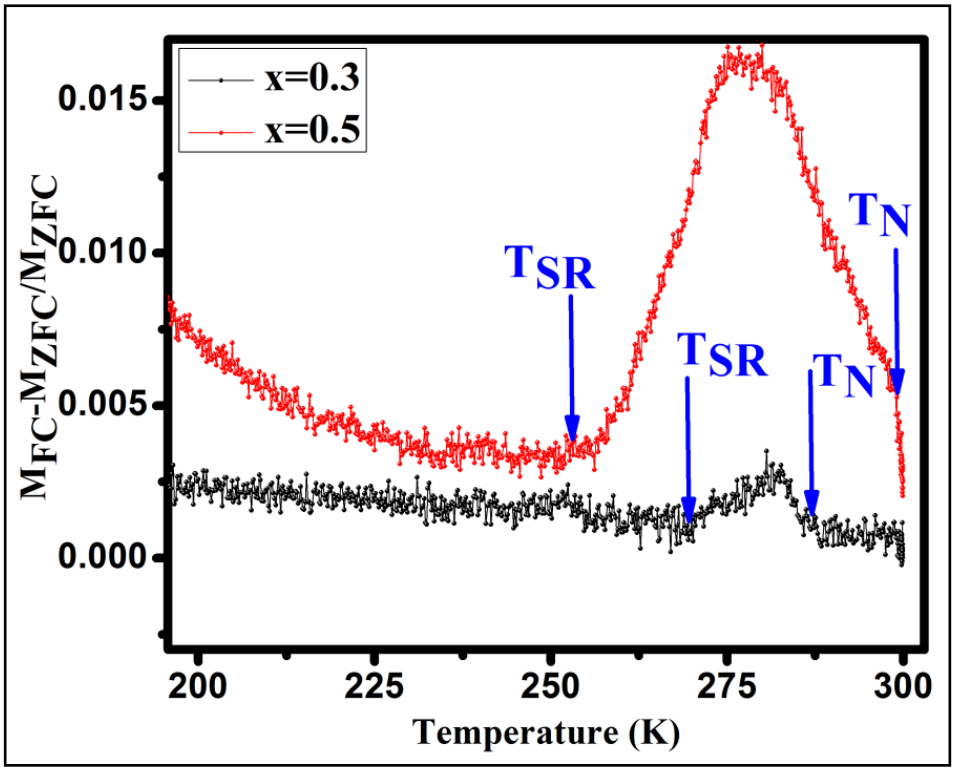

Figure 4.15 *Irreversibility magnetization vs temperature for x = 0.3 and 0.5.*

With increasing Fe concentration, kink position shifts to ~ 10 K for x = 0.5. Besides the peak at ~9.8 K, the slope of the curve changes at ~34 K when x = 0.3. The slope at ~34

K is also shifted to ~37 K for x = 0.5 (**figure 4.14**). T_N is found to be ~210 and ~280 for x = 0.3 and 0.5, respectively. T_N observed at 210 K in Fe doped $GdMnO_3$ represents the transition from paramagnetic to incommensurate antiferromagnectic phase, the anomalies at ~34 and ~9.8 K denote the ordering of Mn^{3+} and Gd^{3+} spins, respectively. T_N in the range of 42-45 K has been reported in $GdMnO_3$ compounds by various authors [[21], [22]]. The significant enhancement in T_N observed at x = 0.5, which approaches room temperature is associated with, subtle structural changes. Previously, we have shown that with increasing Fe concentration upto 20%, the static J-T orbital ordering decreases and posses O' orthorhombic structure. Here we have observed that when 'x' increases from 0.3 to 0.5, O' transform to O type orthorhombic structure. Thus x>0.3 the Fe doping can affect the magnetic exchange interaction. Because half filled e_g orbital of Fe^{3+} ion increases at the cost of quarter occupied Mn^{3+} ion, such an occupied electronic state increases the AFM exchange interaction according to Hund's rule. In addition, increase in c/√2 relative to a in x = 0.5 makes the orbital ordering less stable and strengthen the AFM interaction of e_g^2–O–e_g^2 (Fe–O–Fe). Further an increase in Mn/Fe–O–Mn/Fe bond angle corroborates with the enhancement of AFM interaction according to Goodenough-Kanamori (GK) rule [103].

4.3.2 Field dependent magnetization

The magnetization (M) is measured with varying external field (H) below T_N i.e, at 20 and 4 K shown in **figure 4.16**. At 20 K, along with slim loop magnetization linearly increases with increasing field and the linear increase in magnetization at high field, we observe a slim loop which is not saturated upto 70 kOe. The slim loop appears due to canted spins of Mn which decreases with Fe doping as collinear arrangement of spins increases. The area under the loop increases with decreasing the temperature to 4 K. The

maximum magnetization (M_{max}), coercivity (H_c) and remanence (M_r) estimated from hysteresis loops at 4 and 20 K are tabulated in **Table 4. 2.** While M_{max} increases with increase in Fe concentration due to higher moment of Fe^{3+}, H_c and M_r decrease noticeably indicating the collinear AFM behavior.

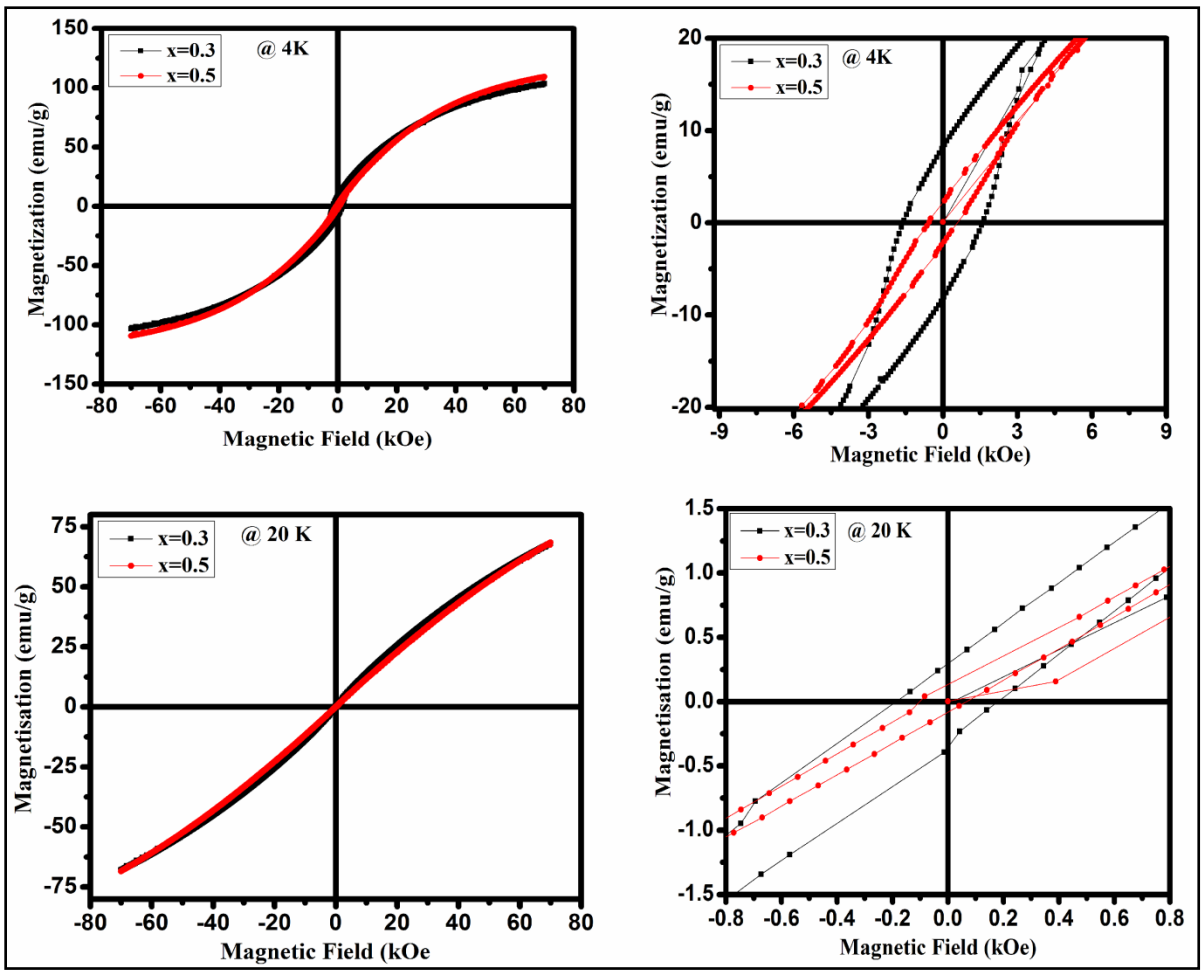

Figure 4.16 *Magnetic field-dependent magnetization at 4 K and 20 K of* $GdMn_{1-x}Fe_xO_3$ *(x = 0.3 and 0.5) and zoom view of Magnetic field-dependent magnetization.*

Table 4.2 Maximium magnetization (M_{max}), remenance (M_r) and coercivity (H_c) for $GdMn_{1-x}Fe_xO_3$ (x = 0.3 and 0.5) at 4 K and 20 K.

Temperature	M_{max}@7 kOe (μ_B)		H_C (kOe)		M_r (μ_B)	
	x = 0.3	x = 0.5	x = 0.3	x = 0.5	x = 0.3	x = 0.5
4 K	4.86	5.12	1.633	0.876	0.37	0.1
20 K	3.17	3.25	0.1914	0.104	0.01	0.006

4.3.3 Temperature dependent ac susceptibility

To investigate the spin dynamics of Fe doped $GdMnO_3$, real ac susceptibility at 31, 101, 299, and 501 Hz in the presence of ac field of 3 Oe has been carried out and is shown in **figure 4.17**. For x = 0.3, the maximum susceptibility appears at ~3.5 K, whereas for x = 0.5, it appears at or below the lowest measurement temperature, i.e., 2 K. Although the shift in in maximum susceptibility with frequency is observed for x = 0.3, for x = 0.5, we could not see such a change due to the limitation of minimum measurement temperature Therefore, to validate the spin glass (SG) behavior in these samples, we have carried out the time dependent remanent magnetization measurement. Further, to validate the SG behavior in these samples, we have carried out the time dependent remanant magnetization measurement.

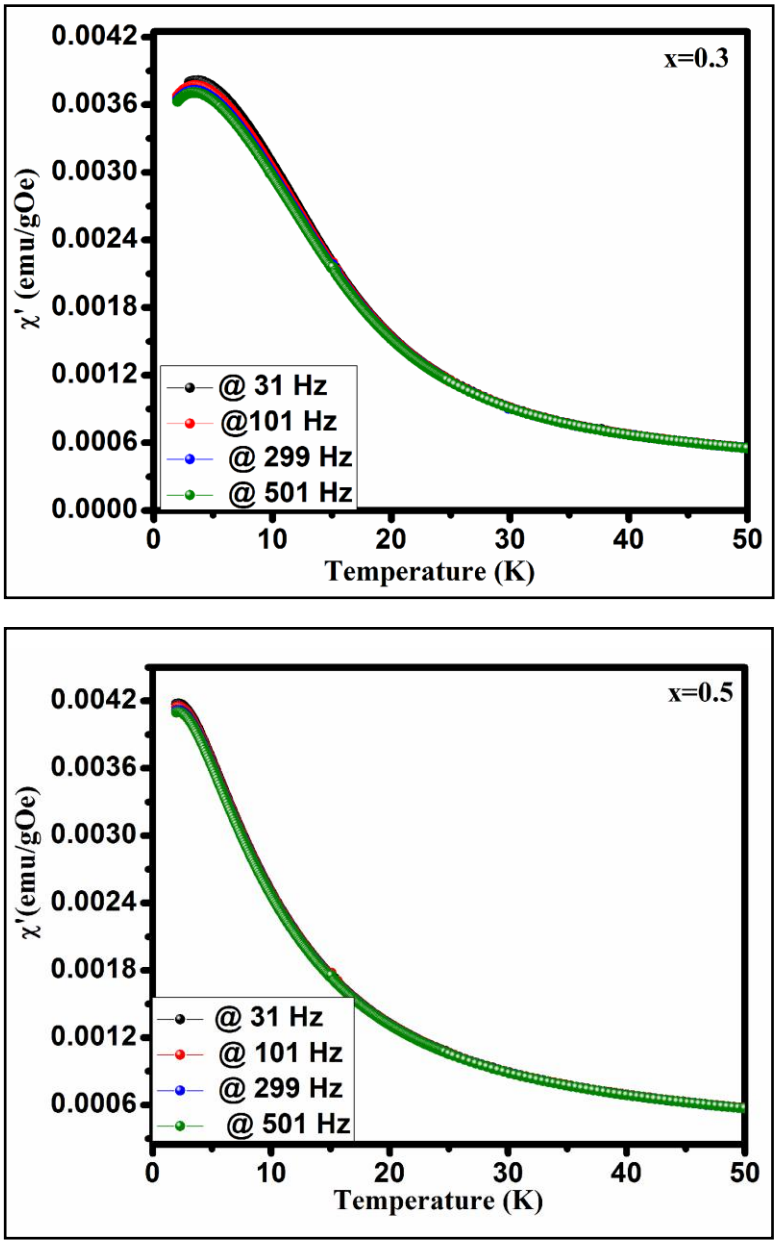

Figure 4.17 *Temperature dependence of the real part of ac susceptibility at various frequencies at the 3 Oe ac field of x = 0.3 and x = 0.5.*

4.3.4 Time dependent magnetization

In this measurement, the sample is cooled from 300 to 2 K in presence of magnetic field of 50 Oe, then the field is removed and the magnetization is recorded as a function of temperature for 3 h. The results are shown as of **figure 4.18**. SG relaxation commonly

follows the power law, $M(t) = M_0 t^{-b}$. In this equation, M_0 (M at t = 0) is initial magnetization and b represents decay parameter which signifies the decay rate [104]. It is clear from fitting that remanent magnetization follows the power law in both samples which confirm the SG like behavior. The SG behavior observed in both samples is attributed to the presence of mixed valency of Mn i.e, Mn^{3+} and Mn^{4+}. Similar spin glass behavior has been reported in K- doped $NdMnO_3$ perovskite [98].

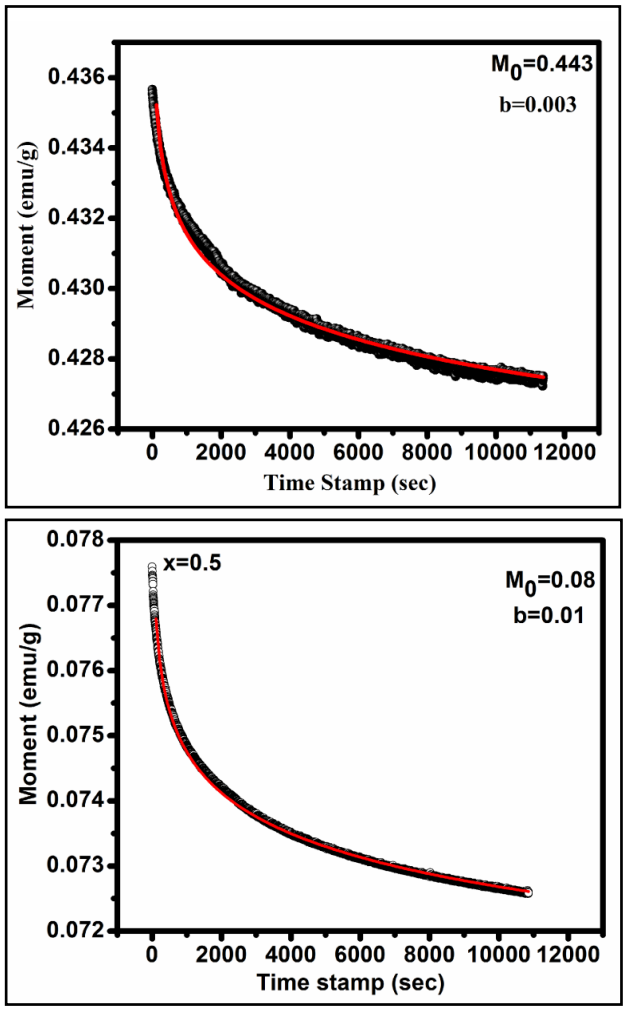

Figure 4.18 *Magnetic relaxation after field cooling in the presence of 50 Oe. The red line shows the fitting to the power law function.*

4.4 Conclusions

In this chapter, the evolution of structure and the rich sequence of magnetic transitions in $GdMnO_3$ nanoparticles synthesized through sol-gel technique after increasing Fe concentration (x) from 0.3 to 0.5. Using XRD, Raman, XPS, PL, magnetization and ac susceptibility measurements, we studied the structural transformation from O' to O type orthorhombic structure along with the reduction in lattice volume. While decrease in lattice volume was contributed by the presence of Mn^{4+}, the structural transformation was attributed to reduction in J-T distortion factor calculated using the bond lengths obtained from Rietveld refinement. Raman spectra confirmed a significant reduction in J-T distortion factor due to decrease in the intensity of asymmetric stretching bonds at 487 and 610 cm^{-1}. Further, the emission peak at ~286 nm in PL spectra disappeared with reduction in J-T distortion factor. PL and XPS both confirmed the presence of Mn^{4+}. PL study demonstrated the emission spectra emerging due to allowed electronic transitions within Mn^{4+} energy bands. Magnetic measurements showed an anomalous increase in T_N to ~ 298 K almost room temperature when '*x*' reached 0.5. While T_N increased with Fe doping, T_{SR} decreased distinctly. The mixed valency of Mn was contributed towards SG behavior observed in both samples.